

Economical ensembles with hypernetworks

João Sacramento^{*,1}, Johannes von Oswald^{*,1}, Seijin Kobayashi^{*,1},
Christian Henning¹, and Benjamin F. Grewe¹

^{*}These authors contributed equally to this work.

¹Institute of Neuroinformatics, University of Zürich, ETH Zürich, Zürich, Switzerland

Correspondence to: `sacramento,oswald,skobayashi@ini.ethz.ch`

Abstract

Averaging the predictions of many independently trained neural networks is a simple and effective way of improving generalization in deep learning. However, this strategy rapidly becomes costly, as the number of trainable parameters grows linearly with the size of the ensemble. Here, we propose a new method to learn *economical* ensembles, where the number of trainable parameters and iterations over the data is comparable to that of a single model. Our neural networks are parameterized by hypernetworks, which learn to embed weights in low-dimensional spaces. In a late training phase, we generate an ensemble by randomly initializing an additional number of weight embeddings in the vicinity of each other. We then exploit the inherent randomness in stochastic gradient descent to induce ensemble diversity. Experiments with wide residual networks on the CIFAR and Fashion-MNIST datasets show that our algorithm yields models that are more accurate and less overconfident on unseen data, while learning as efficiently as a single network.

1 Introduction

Ensembling is a powerful technique to improve predictions and it is essentially applicable to all model classes, including deep neural networks. The predictions of neural network ensembles are often more accurate and more temperate than those produced by single models and they better capture predictive uncertainty for inputs that lie far from the training data [1]. These desirable benefits can be obtained by simply training N models (N *specialists*) independently and then averaging their predictions at test time [2]. With its appealing simplicity, this method comes with an important drawback: it results in a linear increase in parameters and required passes over the data during learning, as well as in test time. Given the current size of deep learning models and datasets, scaling by a factor of N makes ensembling out-of-reach for most practitioners, which simply lack the computational resources [3].

Here, we present an ensembling algorithm that does not require an increase in parameters or training iterations. We therefore classify our approach as *economical*, joining a number of recent other proposals [4–7]. At the heart of our technique is the hypernetwork [8, 9], a neural network which specifies a subset of the parameters of another network from a weight embedding input. To build an ensemble of N models, we introduce a special form of parameter sharing, where every model shares the same hypernetwork. Different models are then specified using N different hypernetwork input embeddings. This results in

extensive parameter sharing across the ensemble – and therefore in potentially large ensemble compression and faster training – since only a tiny fraction of the parameters belongs to each individual model.

Besides providing a new practical and generally applicable algorithm, we present some intriguing results with regards to the compressibility and representation of neural networks in embedding spaces. After learning, we inspect our low-dimensional weight embedding spaces and find a multitude of functionally different high-performance models in the vicinity of each other. Notably, this structured embedding space emerges naturally when learning with stochastic gradient descent (SGD) methods.

We summarize our approach and main contributions below:

- We propose an ensembling algorithm based on hypernetworks, where specialists specify models using low-dimensional embeddings. Every specialist shares the same hypernetwork.
- We introduce late-phase ensembling, where specialist-specific parameters are generated only in late stages of training. We demonstrate that late-phase ensembling is essential to learn economically, i.e., as fast as a single model.
- We investigate a nested optimization algorithm where changes of shared parameters are accumulated over an inner loop, which optimizes each individual specialist. Our experimental work reveals that this nested optimizer can speed-up learning and improve final accuracy.
- Experiments on standard image classification benchmarks show that our economical models display the benefits of large ensembles while staying within the training iterations and numbers of parameters of a single network. We investigate high-performing wide residual networks and find that our economical ensembles achieve state-of-the-art generalization performance. In particular, they (i) are more accurate and score a lower log-likelihood on the held-out test set; and (ii) output less confident predictions on unseen image classes, significantly improving detection of out-of-distribution examples.

2 Economical ensemble learning with hypernetworks

2.1 Hypernetworks

A hypernetwork is a metamodel which generates the parameters of another model. In our work, we follow Ha et al. [8] and consider deterministic hypernetworks which map an embedding vector $\mathbf{e} \in \mathbb{R}^D$ onto the parameters of a primary model, $W = h(\theta, \mathbf{e})$. Here, h is a multivariate real function. Having produced a set of parameters W using the hypernetwork, the primary model then takes over and solves the actual task, generating a prediction $\mathbf{y} = f(W, \mathbf{x})$ for some input pattern \mathbf{x} . In our experiments, we model f as a modern deep neural network. An illustrative diagram can be found in Appendix A.

Hypernetworks can enforce parameter reuse. Instead of producing the entire set of parameters at once, one can partition (or ‘chunk’) W appropriately and then iteratively invoke the same hypernetwork function while selecting different embedding vectors as inputs. In this scheme, embedding vectors can be thought of as generalized parameter location indices, encoded in the real numbers. Since h is differentiable, we can compute gradients end-to-end and learn both the hypernetwork parameters θ as well as the embedding \mathbf{e} itself using the backpropagation algorithm.

Parameter chunking enables compression, since a small hypernetwork can now parameterize a larger primary network. Besides model compression, chunking allows expressing an inductive bias towards

certain patterns of parameter reuse. This holds true even outside compressive regimes. For example, partitioning W layer-by-layer can largely increase the chances of discovering by gradient descent weight configurations that repeat operations over layers, not unlike a recurrent neural network.

Finer partitioning strategies or choosing h to be a multilayer neural network can potentially improve our approach, but require searching over architectures that are harder to optimize. Hence, we restrict our attention to linear hypernetworks and partition our primary network layerwise. For a certain layer l , we generate the primary network weights as

$$W^{(l)} = \theta \mathbf{e}^{(l)},$$

where $\mathbf{e}^{(l)}$ and θ are seen as appropriately shaped tensors, so that their product matches the dimensions of $W^{(l)}$. Since the primary neural networks that we consider in our experiments are not regularly shaped and comprise layers of different dimensions, we simply use a different set of hypernetwork parameters θ for each layer group. We denote by Θ the entire set of hypernetwork parameters.

2.2 Modeling ensembles with shared hypernetworks

Designing an economical ensemble with extensive parameter sharing is challenging. To reap the benefits of ensembling, the set of functions $\{f_i(\mathbf{x})\}_{i=1}^N$ that the ensemble comprises ideally produces diverse outputs for fixed \mathbf{x} , but this is difficult to achieve when most parameters in W are equal.

We propose to address this problem at the metamodeling level. When modeling neural network weights explicitly, parameter sharing amounts to tying a subset of the weights. Here, we generate every weight in W through a hypernetwork and share instead the hypernetwork parameters θ across the ensemble. Then, we grant the i -th specialist its own set of embedding vectors, $E_i = \{\mathbf{e}_i^{(l)}\}_{l=1}^L$. In other words, we give each specialist the freedom to model distinct $f_i(\mathbf{x})$, by picking distinct linear combinations of a shared set of meta-level features in θ . How economical the resulting ensemble is now depends on a hyperparameter, the weight embedding space dimension D . In our ensembles, every specialist i contributes with equal weight to the final prediction, $f(\mathbf{x}) = \frac{1}{N} \sum_{i=1}^N f_i(\mathbf{x})$.

By sharing hypernetworks across multiple layers it is possible to compress modern deep neural networks while preserving final classification accuracy [8]. For moderate compression factors, this form of parameter sharing can sometimes even lead to better predictive models [10]. In our work, we reuse a shared hypernetwork over multiple models, by learning many embedding vectors in parallel. Thus, we seek compression not over the number of parameters of a single model, but over the total number of parameters of an ensemble of multiple models.

2.3 Parameter optimization

In our experiments, we study classification problems. Therefore, to produce probability distributions over classes we employ primary neural networks with softmax output layers. We then minimize the negative log-likelihood on a training dataset. For a given dataset $\mathcal{D} = \{(\mathbf{x}^{(d)}, y^{(d)})\}_{d=1}^{N_D}$ we define our loss function $\mathcal{L}(\mathcal{D})$ to be the cross-entropy between the actual neural network output $f(\mathbf{x})$ and the desired class label y , averaged over examples. Our models are optimized end-to-end with minibatch SGD, by randomly subsampling a minibatch \mathcal{M} of size $N_M = 128$ from \mathcal{D} . This yields the standard loss function $\mathcal{L}(\mathcal{M}, W) = -\frac{1}{N_M} \sum_{d=1}^{N_M} \ln[f(W, \mathbf{x}^{(d)})]_{y^{(d)}}$. Gradients are computed by backpropagation of error using the automatic differentiation software library PyTorch [11]. We use Nesterov momentum [12] and weight

decay, as described in Appendix A.

Stochastic gradients. Besides leading to remarkably efficient optimization [13, 14], the randomness in SGD plays a further crucial role in our ensemble learning algorithm. To learn multiple, diverse specialists, we take advantage of the stochasticity in SGD updates to decorrelate embedding vectors E_i across the ensemble ($i = 1, \dots, N$). This leads to a rather simple procedure: randomly pick a specialist i , randomly sample a minibatch \mathcal{M} , measure the loss $\mathcal{L}(\mathcal{M}, W_i)$ and update parameters using SGD.

Algorithm 1: Nested SGD

Require: Shared parameters Θ ,
specialist parameters $\{E_i\}_{i=1}^N$, dataset \mathcal{D} ,
learning rate η

```

1 for  $1 \leq i \leq N$  do
2    $\mathcal{M}_i \leftarrow$  Sample minibatch from  $\mathcal{D}$ 
3    $E_i \leftarrow E_i - \eta \nabla_{E_i} \mathcal{L}(\mathcal{M}_i, \Theta, E_i)$ 
4    $\Delta\Theta^{(i)} \leftarrow -\eta \nabla_{\Theta} \mathcal{L}(\mathcal{M}_i, \Theta, E_i)$ 
5  $\Theta \leftarrow \Theta + \sum_{i=1}^N \Delta\Theta^{(i)}$ 

```

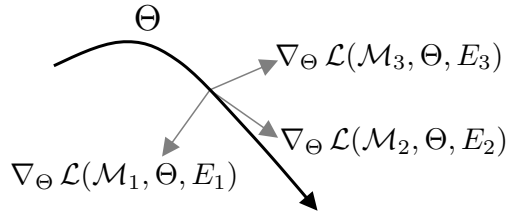


Figure 1: Nested SGD can dampen specialist-to-specialist fluctuations when changing the parameters of shared hypernetworks.

Nested SGD. Being shared across the ensemble, the hypernetwork parameters Θ are bound to receive conflicting update directions in contiguous optimization steps, since a different specialist is picked every time. To stabilize shared parameter updates we investigate a gradient accumulation strategy proposed by Lee et al. [15], which bears some superficial similarity to the MAML algorithm [16]. Instead of updating the hypernetwork parameters Θ concurrently with the specialist-specific embeddings E_i , we withhold changes to Θ until an inner-loop running over every specialist has been concluded. Nesting specialist-specific parameter updates inside shared parameter updates results in a larger effective minibatch of size $N N_M$ when estimating hypernetwork weight gradients. This can dampen specialist-to-specialist fluctuations in $\Delta\Theta$ (Fig. 1). We summarize a single nested SGD iteration in Algorithm 1, with Nesterov momentum disabled for brevity.

Averaged SGD. We also perform experiments with Polyak-averaged SGD [ASGD; 17], which amounts to maintaining a recursively-computed average of SGD updates in time. Polyak-averaged SGD is a well-known optimization algorithm which enjoys accelerated convergence near an optimum [18]. Averaging stochastic weight updates has been recently derived from an objective function that emphasizes flat minima [19], which are in principle more robust to model perturbations [20]. Averaged SGD turns out to improve generalization in deep learning and indeed lead to flatter regions in weight space [21]. We hypothesize that the flatness-seeking behavior of averaged SGD is particularly beneficial when trying to find a consensus among specialists in how to use shared hypernetworks.

2.4 Late-phase ensembling

Ongoing studies of the nonconvex, high-dimensional loss functions that arise in deep learning point to the existence of dense clusters of connected solutions that are accessible by SGD [5, 6, 22]. Indeed, the eigenspectrum of the loss Hessian evaluated at weight configurations found by SGD reveals a large number of directions of low curvature [19, 23]. Although the reasons are not completely understood, this appears to be a recurring phenomenon [24] in overparameterized nonlinear problems. Being robust to

model perturbations, at least along certain directions, is linked to compressibility and an argument can be made for better generalization [20, 25; but see 26].

These considerations led us to explore a perturbative approach to obtain an economical ensemble. Instead of training N specialists from the onset, we first train a single base model with weights W_0 , parameterized by a single set of base embeddings E_0 . After T_0 epochs, a hyperparameter of our algorithm, we generate an ensemble by initializing our set of N specialist embeddings around E_0 . We opt for a simple symmetric Gaussian initialization model. For a given layer l ,

$$\mathbf{e}_i^{(l)} = \mathbf{e}_0^{(l)} + \frac{\sigma \|\mathbf{e}_0^{(l)}\|}{\sqrt{D}} \boldsymbol{\epsilon}_i^{(l)},$$

where the components of $\boldsymbol{\epsilon}_i^{(l)}$ are standard normal variates, σ is a hyperparameter controlling the noise amplitude and the normalization ensures scale-invariance over layers. This initialization is not equivalent to isotropic noise in weight space. Rather, our exploration noise has a linearly deformed and degenerate covariance matrix. We obtain an array of N weight perturbations δW_i with covariance $\sigma^2 \theta \theta^T$ times a normalizing scale factor, where the hypernetwork weights θ are here seen in matrix form, with the columns of θ corresponding to flattened weight tensor features. Furthermore, since D is tiny (θ is a skinny matrix), the majority of the dimensions in W -space will not be explored.

The above algorithm rests upon a number of conjectures. First, we assume that in late stages of learning the base primary model weights W_0 found by SGD can be stochastically perturbed without great increase in the loss. Random δW_i are likely not immediately useful; however, we let SGD adapt both Θ and E to recover from the perturbation. Second, we assume that in the vicinity of the base model weights W_0 produced by E_0 there exist solutions that generate diverse predictions. In other words, we expect our shared hypernetwork ‘weight features’ to be recombinable, without extensive relearning. Our hypothesis is that this algorithm can find a diverse ensemble more economically than when training N specialists from scratch.

3 Experiments

We conduct experiments on standard benchmarks to investigate whether our economical ensembles lead to improved predictive accuracy and uncertainty representation¹. While developing our method, scalability to real-world problems was one of our main concerns. We therefore examine relatively large deep neural networks, which can nonetheless still fit on a modern graphics processing unit. We report mean and standard deviation across three random seeds for our results.

Visual tasks. We train our models to solve three image classification tasks: (i) Fashion-MNIST [27], (ii) CIFAR-10 [28] and (iii) CIFAR-100 [28]. We apply a sequence of standard data preprocessing and augmentation procedures as described in Appendix B. We report prediction accuracy on the standard heldout test sets.

Out-of-distribution detection. We further investigate if our ensembles can represent model uncertainty, and whether their predictions are overconfident, by carrying out a series of out-of-distribution detection (OOD) experiments. OOD is a problem of practical importance, where examples from the test set have to

¹Source code is available under <https://github.com/seijink/e-hyper>

be discriminated from images taken from a variety of classes that the model was not exposed to during learning [29]. Ideally, uncertainty should be high for these novel images. We measure the uncertainty in the predictive distribution $f(\mathbf{x})$ using Shannon’s entropy [30] and evaluate OOD performance using the area under the receiver operating characteristics curve (AUROC).

Wide residual networks. We employ wide residual networks (WRNs) [31, 32] as the base models generated by our hypernetworks, with depth 28 and widening factor 10, a high-performing model for the datasets we consider. WRNs contain regularly shaped layer groups; each group is parameterized by a shared hypernetwork. To accommodate convolutional layers of irregular input and output channel size, we further perform basic partitioning within layers. Specifically, we split the parameters of some convolutional layers along the input channels by a suitable factor, which we choose to be 2. Since the last layer contains few parameters (640 times the number of classes) and because there is no obvious way of partitioning it, we do not compress it using a hypernetwork. When learning with ASGD, we use the same learning rate schedule as [33] and linearly decrease the rate from epoch 80 to 160 (with final rate $\eta = 0.05$). For SGD we replicate the annealing of [31] and multiply the learning rate by 0.2 at epochs 60, 120 and 160. Our initial learning rate is always set to $\eta = 0.1$.

Economical learning. We study a strictly economical learning regime. To that end, we design our hypernetworks so that the number of parameters in an ensemble of size N approximately matches the number of parameters of the corresponding base WRN, at $N = 1$. Furthermore, we fix the number of training epochs to 200, a standard choice for WRN learning on the CIFAR-10/100 and Fashion-MNIST datasets. Our ensemble has $35\,892\,789 + 25\,013\,N$ parameters, while the base WRN has $36\,479\,194$ parameters. We adapt the embedding dimension D per layer group (see Appendix A for the exact numbers). Summed across every layer, our parameterization results in a total embedding size of 654 per specialist.

Methods and models we compare to. Besides comparing to the baseline WRN, we consider our own single model ($N = 1$), which differs in initialization and can behave differently, as the weights are hypernetwork-generated. As described in Section 2.3 we optimize our models with both SGD and averaged SGD, following Izmailov et al. [21]. We then consider (non-economical) independently-trained ensembles [IEs; 1] as well as snapshot ensembles [SEs; 5] and fast geometric ensembles [FGEs; 6], two alternative economical methods. In SEs, specialists are created by collecting weights along the path to a solution, while FGEs exploit certain geometrical regularities of the loss function. We generate SEs with averaged SGD to boost its performance and capture equally-spaced snapshots after epoch 164, albeit without a cyclical learning rate, for comparability with the remaining methods. Additionally, we experiment with SWAG [33] (we draw $N = 30$ weight samples, the authors’ recommended choice). SWAG represents model uncertainty [34] using an approximate parameter covariance matrix and is therefore more sophisticated than a diagonal Gaussian approximation [35], while being able to scale to the large WRNs we consider here.

3.1 Test set accuracy

We first study generalization on the held-out test set. We report results obtained with averaged SGD (see Appendix C for additional experiments with SGD) and our late-phase ensembling (epoch $T_0 = 120$), with initialization noise $\sigma = 0.25$. The remaining hyperparameters are detailed in Appendix B.

Table 1: Test set accuracies (in %) when training (for 200 epochs except IEs) on Fashion-MNIST (*FM*) and CIFAR-10/100 (*C10*, *C100*). The predictive accuracy of the baseline (*Ours* $N=1$, learned with ASGD) is significantly improved using our ensembling method (*Ours*, learned with nested ASGD, $N=10$), outperforming three other state-of-the-art economical methods (*SWAG*, *FGE*, *SE*). FGE results ($N=12$) from [6]. Best results in boldface, excluding non-economical IEs (single seed).

	WRN ($N=1$)	Ours ($N=1$)	Ours	SWAG	FGE	SE	IE
FM	95.61 \pm 0.08	95.56 \pm 0.08	95.80 \pm 0.03	95.42 \pm 0.06	—	95.62 \pm 0.09	95.79
C10	96.46 \pm 0.05	96.45 \pm 0.03	96.79 \pm 0.07	96.17 \pm 0.09	96.35 \pm 0.1	96.34 \pm 0.14	96.70
C100	82.58 \pm 0.08	82.51 \pm 0.03	83.03 \pm 0.33	82.13 \pm 0.03	82.3 \pm 0.2	82.56 \pm 0.47	83.62

Table 2: Final ensemble test set classification accuracy (in %) when $N = 10$. We compare averaged SGD to nested averaged SGD, with learning rate scheduling and while learning at constant high learning rate ($\eta = 0.1$ fixed). Nested SGD (*NASGD*) leads to a consistent improvement in predictive accuracy, when compared to averaged SGD alone (*ASGD*) on Fashion-MNIST and CIFAR-10/100.

	ASGD (constant LR)	NASGD (constant LR)	ASGD	NASGD
FM	91.12 \pm 1.69	94.87 \pm 0.02	95.58 \pm 0.05	95.80 \pm 0.03
C10	95.57 \pm 0.18	96.73 \pm 0.10	96.44 \pm 0.05	96.79 \pm 0.07
C100	81.80 \pm 0.24	82.91 \pm 0.40	82.76 \pm 0.24	83.03 \pm 0.33

We find that the predictive accuracy of our base model ($N = 1$) is improved when raising the number of specialists to $N = 10$, cf. Table 1. Our economical ensembles outperform SWAG, FGE and SE. This is a notable result, as all three methods are strong recent contenders on the CIFAR datasets. Moreover, our experiments confirm that nested SGD (Algorithm 1), when applied to our ensembles with strong parameter sharing, can accelerate learning (Fig. 2) and improve generalization (Table 2). For test set results on larger WRN models with an additional data augmentation procedure (cutout; [36]), we refer to Appendix C.

Additionally, we run a set of experiments on Fashion-MNIST and CIFAR-10/100 to examine learning at constant high rate. We disable annealing altogether and fix the learning rate to $\eta = 0.1$. Strikingly, we find that nested averaged SGD incurs little to essentially no penalty on final test set accuracy (Table 2). This result is strong evidence for the stabilizing effect of nested SGD, hinting to flat-minima seeking behavior and a possible connection to entropy SGD [19].

3.2 Out-of-distribution detection

Next, we study OOD performance when training on CIFAR-10/100 and drawing novel images at test time from the SVHN [37], LSUN [38] and Tiny ImageNet datasets, as well as from the corresponding other CIFAR dataset, following the exact preprocessing described by Lee et al. [39]. Results obtained when learning on Fashion-MNIST can be found in Appendix C.

Our hyperparameter search (see Appendix C) reveals that increased levels of specialist initialization noise σ are beneficial in OOD problems and that nested SGD is not, staying in between SGD and averaged SGD alone; we speculate that reducing the noisiness of the trajectory to a solution leads to less diversity in

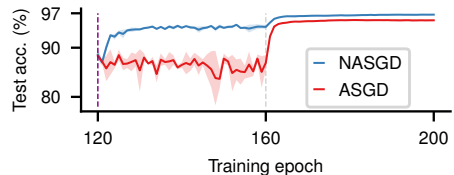


Figure 2: Ensemble test accuracy as training proceeds (CIFAR-10, $N = 10$, constant $\eta = 0.1$). The ensemble is created at $T_0 = 120$ and ASGD enabled at epoch 160. Nested ASGD accelerates convergence and improves final accuracy.

Table 3: Test set accuracy (in %) and OOD performance, measured by the AUROC ($\times 100$). We train our models (200 epochs, SGD and ASGD) on CIFAR-10 (C10) and CIFAR-100 (C100) and attempt to discriminate test set images from novel ones drawn from the SVHN, LSUN, Tiny ImageNet (TIN) and the resp. other CIFAR dataset. Our ensembles (*Ours*, $N=10$) significantly improve the $N=1$ baseline and outperform all other economical ensembling methods considered here. Late-phase ensembling is crucial in improving against $N=1$, as evidenced by the poor result obtained when learning every specialist from scratch (*scratch*). Best results in boldface, excluding non-economical IEs (single seed).

Data	Optim.	Method	Test acc.	SVHN	LSUN	TIN	CIFAR	
C10	SGD	WRN ($N=1$)	96.01 \pm 0.09	94.08 \pm 0.02	93.32 \pm 1.11	90.22 \pm 1.17	88.70 \pm 0.21	
		Ours ($N=1$)	96.08 \pm 0.16	93.30 \pm 1.59	91.68 \pm 0.25	87.85 \pm 2.09	87.70 \pm 0.57	
		Ours	96.06 \pm 0.17	95.56 \pm 1.81	95.96 \pm 0.60	93.99 \pm 0.77	89.22 \pm 0.62	
		IE	96.83	97.52	95.74	93.19	92.10	
	ASGD	WRN ($N=1$)	96.46 \pm 0.05	97.91 \pm 0.94	96.91 \pm 0.09	95.53 \pm 0.20	92.90 \pm 0.07	
		Ours ($N=1$)	96.45 \pm 0.03	98.63 \pm 0.24	97.03 \pm 0.10	95.69 \pm 0.43	93.02 \pm 0.02	
		Ours (scratch)	96.42 \pm 0.14	98.36 \pm 0.18	96.45 \pm 0.66	94.50 \pm 0.99	90.76 \pm 0.33	
		SWAG	96.17 \pm 0.09	98.25 \pm 0.15	97.48 \pm 0.23	95.77 \pm 0.43	92.86 \pm 0.09	
		SE	96.34 \pm 0.14	98.20 \pm 1.08	96.92 \pm 0.46	95.32 \pm 0.65	92.52 \pm 0.31	
		Late IE	95.96 \pm 0.11	98.30 \pm 0.15	96.77 \pm 0.27	94.84 \pm 0.32	92.70 \pm 0.06	
		Ours	96.48 \pm 0.02	99.07 \pm 0.04	97.53 \pm 0.04	96.11 \pm 0.13	93.36 \pm 0.15	
		IE	96.70	98.45	97.60	98.26	93.43	
	C100	SGD	WRN ($N=1$)	80.68 \pm 0.4	78.84 \pm 1.20	77.64 \pm 3.64	75.46 \pm 2.61	80.75 \pm 0.34
			Ours ($N=1$)	80.54 \pm 0.45	79.43 \pm 5.31	81.19 \pm 2.37	79.71 \pm 2.45	80.74 \pm 0.42
Ours			80.87 \pm 0.32	82.46 \pm 5.27	84.55 \pm 1.92	81.45 \pm 1.80	81.71 \pm 0.15	
IE			83.46	85.21	84.37	88.38	83.10	
ASGD		WRN ($N=1$)	82.58 \pm 0.08	84.92 \pm 1.40	79.61 \pm 2.40	79.11 \pm 3.28	81.18 \pm 0.22	
		Ours ($N=1$)	82.51 \pm 0.03	86.95 \pm 2.25	83.84 \pm 1.08	81.91 \pm 0.94	81.69 \pm 0.25	
		Ours (scratch)	81.97 \pm 0.11	84.69 \pm 2.97	78.92 \pm 4.10	75.97 \pm 3.55	79.60 \pm 1.02	
		SWAG	82.12 \pm 0.03	82.37 \pm 1.24	83.85 \pm 5.40	83.51 \pm 4.12	81.58 \pm 0.37	
		SE	82.56 \pm 0.47	84.79 \pm 3.44	76.98 \pm 7.17	78.31 \pm 4.90	81.26 \pm 0.38	
		Late IE	82.54 \pm 0.06	84.93 \pm 0.62	80.29 \pm 1.66	79.02 \pm 1.69	81.42 \pm 0.09	
		Ours	82.55 \pm 0.13	86.67 \pm 1.28	86.58 \pm 2.96	85.54 \pm 3.01	81.71 \pm 0.23	
		IE	83.62	85.79	83.45	82.48	82.48	

the embedding space. We choose to report here the optimal configuration for OOD, that we stress is a different one from the best test set configuration from Section 3.1. Here, $\sigma = 0.5$, nested SGD is not used, and a single set of batch normalization units [40] is shared over the ensemble. As before, the ensemble is initialized at $T_0 = 120$.

At $N = 10$, our economical ensembles achieve lower test set negative log-likelihood (Table 4), which is routinely used to assess predictive uncertainty [41, 1, 33]. We also find that their predictions are significantly less confident when presented with novel images, as reflected by the higher AUROC scores achieved across datasets (Table 3). It is also interesting to note that there is a large performance gap between models trained with and without averaged SGD. These results on OOD problems complement the recently observed improved test set generalization achieved by averaged SGD [21].

We also confirm the importance of late-phase ensembling in achieving improvements within our strictly-economical regime. When using the exact same hyperparameters but learning every specialist from the start (*scratch*, Table 3), the resulting ensemble is not even able to reach baseline performance ($N = 1$). Interestingly, a non-economical control consisting of a full-fledged ensemble of the base WRN (with N times more parameters), late-phase generated at T_0 ($\sigma = 0.5$) and then onwards independently trained (*Late IE*, Table 3), is also not as strong as our method. This holds true irrespective of whether we apply our noisy initialization (here, directly in weight space) or not. This speaks for the efficiency of learning models that are represented compressively in embedding spaces.

Embedding space visualization. Finally, we examine the weight embedding space after learning. We construct a plane which passes through the embeddings of three specialists chosen at random and visualize the test set accuracy as we explore in this plane (Fig. 3, additional samples as well as the training and test log-likelihoods in Appendix C). This analysis reveals a surprisingly rich embedding structure induced by our concurrent stochastic learning of multiple specialists. We find that our embeddings are not isolated, nor separated by ridges, but are rather positioned in a basin rich in high-performance solutions, with a local elliptical contour geometry that reveals robustness to perturbations along certain directions [19, 21, 24, 20].

4 Discussion

Stochastic weight embeddings. Stochastic hypernetworks [42–45] draw samples from very high-dimensional weight distributions, typically learned to approximate the Bayesian posterior $p(W | \mathcal{D})$. Often, this involves solving variational problems that are presently challenging at scale [46]. Recent work suggests restricting inference to the low-dimensional embedding space while keeping the remaining parameters fixed [47]. With our ensemble learning algorithm, we seek a discrete set of N weight configurations which are obtained by log-likelihood maximization. This is a more modest goal that is commonly met in deep learning and it is why we were able to study relatively large models in our experiments. Thanks to the efficiency of SGD, it is plausible to assume that our approach will scale to even larger problem instances.

Table 4: Test set negative log-likelihood on CIFAR-10/100, ASGD learning.

	Ours ($N=1$)	Ours ($N=10$)
C10	1125 \pm 9	1081 \pm 4
C100	6848 \pm 127	6259 \pm 177

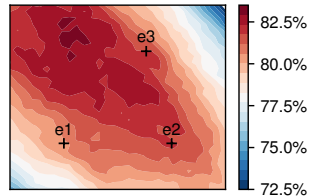


Figure 3: Test set accuracy on a plane given by the affine combination of 3 specialist embeddings (CIFAR-100, post-learning).

Related economical ensembling methods. Dropout is a widespread regularizer which can be seen as an economical ensembling method: multiplying activations with Bernoulli masks amounts to sampling from a large number of networks (exponential in the number of neurons) that share all parameters [48, 4]. We did not explore the use of dropout, but, at least in principle, our methods are not exclusive and it is straightforward to combine them. We did however partially employ another economical ensembling technique. To better accommodate for the different predictions of each model we used specialist-specific batch normalization units in some of our experiments (see Appendices B and C for more details and controls). This introduces a separate set of multiplicative scale factors per specialist. Such scaling is similar, though not equivalent, to an elementwise multiplication of weights by rank-1 masks, an ensembling method that has been recently proposed [7].

Ensemble diversity. We rely on stochastic initialization and gradient noise to induce diversity across specialists, but it is possible to incorporate additional mechanisms. One possibility is to directly anticorrelate the predictive distributions with a regularizer, a standard technique in ensemble learning [49]. Another option is to regularize in weight embedding space instead, for example by encouraging embeddings to move towards orthogonal configurations.

Complementary methods. A number of existing complementary methods can be applied in a straightforward way to our economical ensembles. For example, to name a few: (i) temperature scaling, a surprisingly effective calibration algorithm [50]; (ii) stochastic and adversarial data augmentation strategies, that are known to improve OOD performance [1, 51]; (iii) other choices of classifiers beyond a simple linear-softmax layer [39]; (iv) multiplicative (dropout) noise [48], applied solely to embedding vectors, to prevent excessive co-tuning of embedding patterns and the corresponding hypernetwork parameters. If violating our economical learning desiderata is acceptable, it is even possible to train a full-fledged ensemble, where each model is one of our economical ensembles.

Slower inference. Test-time inference is slower for ensembles due to the averaging over specialists. A surprisingly effective approach is to distill the ensemble-averaged predictive distribution into a single model [52, 53]. Alternatively, we could elect a single weight embedding set E^* as representative of the ensemble and sidestep the additional learning required by distillation. Exploring representative election algorithms – essentially a compressed model search in embedding space – is in our eyes an exciting future work direction.

Learning reusable primitives by gradient descent. Hypernetwork learning can be seen as a greedy gradient-based search for reusable computational primitives. Methodological differences aside, our goals are not far from those of neuroevolution algorithms [54]. As evolution did for brains, the discovery of a set of canonical primitives that enable learning, small enough to be encoded in a genome, is a fundamental open problem which could arguably bring us closer to understanding biological learning [55–57]. It has been recently demonstrated that hypernetworks can discover computations that repeat over layers [8, 10] and tasks [58–60]. Here, we have shown that a set of specialists can learn to reuse a shared hypernetwork, while expressing different predictions over the same data. Our results therefore represent further evidence that, with the right architectural biases, reusable computations can be harnessed and discovered by a method as simple as SGD.

5 Conclusion

We examined a new economical ensemble learning method based on hypernetworks. Using hypernetworks allowed us to simultaneously learn different models in a compressed low-dimensional weight embedding space. This way, we were able to avoid the increase in parameters that is associated with conventional ensembling, which is often too costly. Despite its economical character, our algorithm achieved compelling improvements in both prediction accuracy and predictive uncertainty modeling on standard deep learning benchmarks. Notably, this was possible without requiring any extra training iterations. The method we propose is scalable and simple to implement, and could therefore be of practical interest.

Acknowledgements

This work was supported by the Swiss National Science Foundation (B.F.G. CRSII5-173721 and 315230_189251), ETH project funding (B.F.G. ETH-20 19-01), the Human Frontiers Science Program (RGY0072/2019) and funding from the Swiss Data Science Center (B.F.G. C17-18, J.v.O. P18-03). J.S. was supported by an Ambizione grant (PZ00P3_186027) from the Swiss National Science Foundation. We thank Alexander Meulemans, Nicolas Zucchet, Simon Schug and Xu He for thoughtful comments on the manuscript.

References

- [1] Balaji Lakshminarayanan, Alexander Pritzel, and Charles Blundell. Simple and scalable predictive uncertainty estimation using deep ensembles. In *Advances in Neural Information Processing Systems 30*. 2017.
- [2] L.K. Hansen and P. Salamon. Neural network ensembles. *IEEE Transactions on Pattern Analysis and Machine Intelligence*, 12(10):993–1001, October 1990.
- [3] Rohan Anil, Gabriel Pereyra, Alexandre Passos, Robert Ormandi, George E Dahl, and Geoffrey E Hinton. Large scale distributed neural network training through online distillation. *arXiv preprint arXiv:1804.03235*, 2018.
- [4] Yarín Gal and Zoubin Ghahramani. Dropout as a Bayesian approximation: representing model uncertainty in deep learning. In *International Conference on Machine Learning*, pages 1050–1059, June 2016.
- [5] Gao Huang, Yixuan Li, Geoff Pleiss, Zhuang Liu, John E. Hopcroft, and Kilian Q. Weinberger. Snapshot ensembles: train 1, get M for free. In *International Conference on Learning Representations*, March 2017.
- [6] Timur Garipov, Pavel Izmailov, Dmitrii Podoprikin, Dmitry P Vetrov, and Andrew G Wilson. Loss surfaces, mode connectivity, and fast ensembling of DNNs. In *Advances in Neural Information Processing Systems 31*. 2018.
- [7] Yeming Wen, Dustin Tran, and Jimmy Ba. Batchensemble: an alternative approach to efficient ensemble and lifelong learning. *arXiv preprint arXiv:2002.06715*, February 2020.

- [8] David Ha, Andrew M. Dai, and Quoc V. Le. Hypernetworks. In *International Conference on Learning Representations*, 2017.
- [9] Jürgen Schmidhuber. Learning to Control Fast-Weight Memories: An Alternative to Dynamic Recurrent Networks. *Neural Computation*, 4(1):131–139, January 1992.
- [10] Pedro Savarese and Michael Maire. Learning implicitly recurrent CNNs through parameter sharing. In *International Conference on Learning Representations*, 2019.
- [11] Adam Paszke, Sam Gross, Francisco Massa, Adam Lerer, James Bradbury, Gregory Chanan, Trevor Killeen, Zeming Lin, Natalia Gimelshein, Luca Antiga, Alban Desmaison, Andreas Kopf, Edward Yang, Zachary DeVito, Martin Raison, Alykhan Tejani, Sasank Chilamkurthy, Benoit Steiner, Lu Fang, Junjie Bai, and Soumith Chintala. PyTorch: an imperative style, high-performance deep learning library. In *Advances in Neural Information Processing Systems* 32. 2019.
- [12] Yurii Nesterov. *Introductory lectures on convex optimization: a basic course*. Springer US, 2004.
- [13] Léon Bottou and Olivier Bousquet. The tradeoffs of large scale learning. In *Advances in Neural Information Processing Systems* 20. 2008.
- [14] Stephan Mandt, Matthew D Hoffman, and David M Blei. Stochastic gradient descent as approximate Bayesian inference. *The Journal of Machine Learning Research*, 18(1):4873–4907, 2017.
- [15] Stefan Lee, Senthil Purushwalkam, Michael Cogswell, David Crandall, and Dhruv Batra. Why M heads are better than one: training a diverse ensemble of deep networks. *arXiv preprint: arXiv:1511.06314*, November 2015. arXiv: 1511.06314.
- [16] Chelsea Finn, Pieter Abbeel, and Sergey Levine. Model-agnostic meta-learning for fast adaptation of deep networks. In *International Conference on Machine Learning*, pages 1126–1135, July 2017.
- [17] Boris T Polyak and Anatoli B Juditsky. Acceleration of stochastic approximation by averaging. *SIAM Journal on Control and Optimization*, 30(4):838–855, 1992.
- [18] Léon Bottou. Large-scale machine learning with stochastic gradient descent. In *Proceedings of COMPSTAT’2010*, pages 177–186. Springer, 2010.
- [19] Pratik Chaudhari, Anna Choromanska, Stefano Soatto, Yann LeCun, Carlo Baldassi, Christian Borgs, Jennifer Chayes, Levent Sagun, and Riccardo Zecchina. Entropy-SGD: Biasing gradient descent into wide valleys. *Journal of Statistical Mechanics: Theory and Experiment*, 2019(12):124018, 2019.
- [20] Sepp Hochreiter and Jürgen Schmidhuber. Flat minima. *Neural Computation*, 9(1):1–42, January 1997. Publisher: MIT Press.
- [21] Pavel Izmailov, Dmitrii Podoprikin, Timur Garipov, Dmitry Vetrov, and Andrew Gordon Wilson. Averaging weights leads to wider optima and better generalization. In *Uncertainty in Artificial Intelligence*, 2018.
- [22] Carlo Baldassi, Fabrizio Pittorino, and Riccardo Zecchina. Shaping the learning landscape in neural networks around wide flat minima. *Proceedings of the National Academy of Sciences*, 117(1): 161–170, January 2020.

- [23] Levent Sagun, Utku Evci, V. Ugur Guney, Yann Dauphin, and Leon Bottou. Empirical analysis of the Hessian of over-parametrized neural networks. *arXiv preprint arXiv:1706.04454*, May 2018.
- [24] Kevin S. Brown and James P. Sethna. Statistical mechanical approaches to models with many poorly known parameters. *Physical Review E*, 68(2):021904, August 2003.
- [25] Nitish Shirish Keskar, Dheevatsa Mudigere, Jorge Nocedal, Mikhail Smelyanskiy, and Ping Tak Peter Tang. On large-batch training for deep learning: generalization gap and sharp minima. In *International Conference on Learning Representations*, 2017.
- [26] Laurent Dinh, Razvan Pascanu, Samy Bengio, and Yoshua Bengio. Sharp minima can generalize for deep nets. In *International Conference on Machine Learning*, pages 1019–1028, August 2017.
- [27] Han Xiao, Kashif Rasul, and Roland Vollgraf. Fashion-MNIST: a novel image dataset for benchmarking machine learning algorithms. *arXiv preprint arXiv:1708.07747*, September 2017.
- [28] Alex Krizhevsky. Learning multiple layers of features from tiny images. Technical report, 2009.
- [29] Dan Hendrycks and Kevin Gimpel. A baseline for detecting misclassified and out-of-distribution examples in neural networks. In *International Conference on Learning Representations*, 2017.
- [30] Thomas M. Cover and Joy A. Thomas. *Elements of Information Theory*. Wiley-Interscience, USA, 2006.
- [31] Sergey Zagoruyko and Nikos Komodakis. Wide residual networks. In Richard C. Wilson, Edwin R. Hancock, and William A. P. Smith, editors, *Proceedings of the British Machine Vision Conference*, 2016.
- [32] Kaiming He, Xiangyu Zhang, Shaoqing Ren, and Jian Sun. Deep residual learning for image recognition. pages 770–778, 2016.
- [33] Wesley J Maddox, Pavel Izmailov, Timur Garipov, Dmitry P Vetrov, and Andrew Gordon Wilson. A simple baseline for Bayesian uncertainty in deep learning. In *Advances in Neural Information Processing Systems 32*. 2019.
- [34] David J. C. MacKay. A practical Bayesian framework for backpropagation networks. *Neural Computation*, 4(3):448–472, 1992.
- [35] John S. Denker and Yann LeCun. Transforming neural-net output levels to probability distributions. In *Advances in Neural Information Processing Systems 3*. 1991.
- [36] Terrance Devries and Graham W. Taylor. Improved regularization of convolutional neural networks with cutout. *arXiv preprint arXiv:1708.04552*, 2017.
- [37] Yuval Netzer, Tao Wang, Adam Coates, Alessandro Bissacco, Bo Wu, and Andrew Y. Ng. Reading digits in natural images with unsupervised feature learning. In *NIPS Workshop on Deep Learning and Unsupervised Feature Learning*, 2011.
- [38] Fisher Yu, Yinda Zhang, Shuran Song, Ari Seff, and Jianxiong Xiao. LSUN: construction of a large-scale image dataset using deep learning with humans in the loop. *arXiv preprint arXiv:1506.03365*, 2015.

- [39] Kimin Lee, Kibok Lee, Honglak Lee, and Jinwoo Shin. A simple unified framework for detecting out-of-distribution samples and adversarial attacks. In *Advances in Neural Information Processing Systems 31*. 2018.
- [40] Sergey Ioffe and Christian Szegedy. Batch normalization: accelerating deep network training by reducing internal covariate shift. In *International Conference on Machine Learning*, 2015.
- [41] Yarin Gal. *Uncertainty in deep learning*. PhD thesis, University of Cambridge, 2016.
- [42] David Krueger, Chin-Wei Huang, Riashat Islam, Ryan Turner, Alexandre Lacoste, and Aaron Courville. Bayesian hypernetworks. *arXiv preprint arXiv:1710.04759*, 2017.
- [43] Nick Pawlowski, Andrew Brock, Matthew C. H. Lee, Martin Rajchl, and Ben Glocker. Implicit weight uncertainty in neural networks. *arXiv preprint arXiv:1711.01297*, 2017.
- [44] Christos Louizos and Max Welling. Multiplicative normalizing flows for variational Bayesian neural networks. In *International Conference on Machine Learning*, 2017.
- [45] Vikranth Dwaracherla, Xiuyuan Lu, Morteza Ibrahimi, Ian Osband, Zheng Wen, and Benjamin Van Roy. Hypermodels for exploration. In *International Conference on Learning Representations*, 2020.
- [46] Léonard Blier and Yann Ollivier. The description length of deep learning models. In *Advances in Neural Information Processing Systems*, 2018.
- [47] Pavel Izmailov, Wesley J. Maddox, Polina Kirichenko, Timur Garipov, Dmitry Vetrov, and Andrew Gordon Wilson. Subspace inference for Bayesian deep learning. In *Uncertainty in Artificial Intelligence*, July 2019.
- [48] Nitish Srivastava, Geoffrey Hinton, Alex Krizhevsky, Ilya Sutskever, and Ruslan Salakhutdinov. Dropout: a simple way to prevent neural networks from overfitting. *The Journal of Machine Learning Research*, 15(1):1929–1958, 2014.
- [49] Y. Liu and X. Yao. Ensemble learning via negative correlation. *Neural Networks*, 12(10):1399–1404, December 1999.
- [50] Chuan Guo, Geoff Pleiss, Yu Sun, and Kilian Q Weinberger. On calibration of modern neural networks. In *International Conference on Machine Learning*, 2017.
- [51] Shiyu Liang, Yixuan Li, and R. Srikant. Enhancing the reliability of out-of-distribution image detection in neural networks. In *International Conference on Learning Representations*, 2018.
- [52] Geoffrey Hinton, Oriol Vinyals, and Jeff Dean. Distilling the knowledge in a neural network. *arXiv preprint arXiv:1503.02531*, 2015.
- [53] Anoop Korattikara Balan, Vivek Rathod, Kevin P Murphy, and Max Welling. Bayesian dark knowledge. In *Advances in Neural Information Processing Systems 28*. 2015.
- [54] Kenneth O. Stanley, Jeff Clune, Joel Lehman, and Risto Miikkulainen. Designing neural networks through neuroevolution. *Nature Machine Intelligence*, 1(1):24–35, January 2019.
- [55] Timothy P. Lillicrap and Konrad P. Kording. What does it mean to understand a neural network? *arXiv preprint arXiv:1907.06374*, July 2019.

- [56] Anthony M. Zador. A critique of pure learning and what artificial neural networks can learn from animal brains. *Nature Communications*, 10(1):3770, August 2019.
- [57] Adam Gaier and David Ha. Weight agnostic neural networks. In *Advances in Neural Information Processing Systems 32*. 2019.
- [58] Andrei A. Rusu, Dushyant Rao, Jakub Sygnowski, Oriol Vinyals, Razvan Pascanu, Simon Osindero, and Raia Hadsell. Meta-learning with latent embedding optimization. In *International Conference on Learning Representations*, 2019.
- [59] Johannes von Oswald, Christian Henning, João Sacramento, and Benjamin F. Grewe. Continual learning with hypernetworks. In *International Conference on Learning Representations*, 2020.
- [60] Andrew K. Lampinen and James L. McClelland. Transforming task representations to allow deep learning models to perform novel tasks. *arXiv preprint arXiv:2005.04318*, May 2020.
- [61] Kaiming He, Xiangyu Zhang, Shaoqing Ren, and Jian Sun. Delving deep into rectifiers: surpassing human-level performance on ImageNet classification. *arXiv preprint arXiv:1502.01852*, February 2015.
- [62] Yann LeCun, Corinna Cortes, and CJ Burges. MNIST handwritten digit database. *ATT Labs*. Available: <http://yann.lecun.com/exdb/mnist>, 2010.
- [63] Tarin Clanuwat, Mikel Bober-Irizar, Asanobu Kitamoto, Alex Lamb, Kazuaki Yamamoto, and David Ha. Deep learning for classical japanese literature. *arXiv preprint arXiv:1812.01718*, 2018.
- [64] Gregory Cohen, Saeed Afshar, Jonathan Tapson, and André van Schaik. EMNIST: Extending MNIST to handwritten letters. pages 2921–2926, May 2017.
- [65] J. D. Hunter. Matplotlib: A 2D graphics environment. *Computing in Science & Engineering*, 9(3): 90–95, 2007.

Appendices

A Network architecture

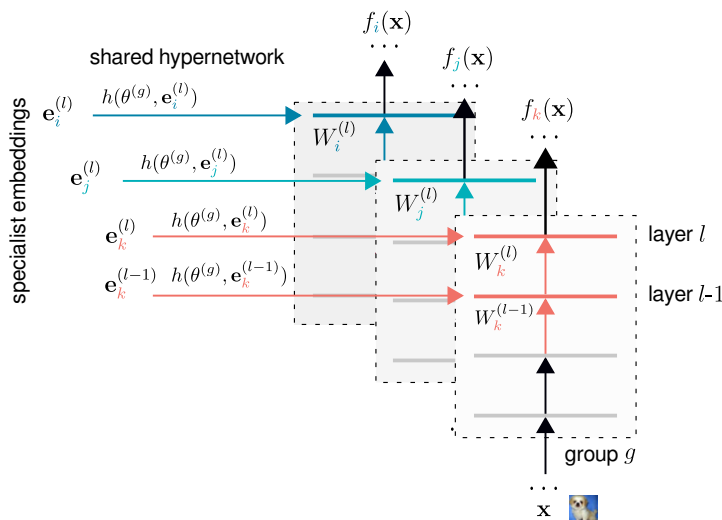


Figure S1: In our economical ensembles, a hypernetwork with parameters $\theta^{(g)}$ is shared across N specialists and within a group of layers g with the same dimensions (dashed area). Every specialist i specifies its weights $W_i^{(l)}$ for some layer l through a low-dimensional weight embedding vector $e_i^{(l)}$. Given an input x , this yields a set of predictions $\{f_i(x)\}_{i=1}^N$. The ensemble prediction $f(x)$ is obtained by averaging over the N specialists. Best seen in color.

The architecture of the primary base model we use on all our experiments is identical to the WRN 28-10 described by Zagoruyko and Komodakis [31]. We do not use dropout or biases in the convolutional layers. The parameters of every convolutional layer are hypernetwork-generated, with one hypernetwork per layer group (Table S1). The remaining parameters, namely those of the batch normalization (batchnorm) units, as well as the final linear layer, are specialist-specific and non-hypernetwork-generated, unless specified otherwise. These parameters, together with the weight embeddings, are used to generate the primary network for each specialist (cf. Fig. S1).

B Hyperparameters and experimental details for main text results

Momentum and weight decay. Regardless of the choice of optimizer, for all experiments reported in the main text we follow the original study of wide residual networks [31] and set Nesterov momentum to 0.9 and weight decay to 0.0005 for all parameters, except weight embeddings, for which decay is turned off. Turning off embedding decay was suggested by Savarese and Maire [10], who similarly studied high-performing linear hypernetwork architectures for WRNs.

Parameter initialization. Following Savarese and Maire [10], we initialize the weight embeddings with a random pseudo-orthogonal initialization over layers. When initializing the ensemble at a late-phase we generate the specialist-specific last-layer weights $W_i^{(L)}$, which are not modeled with a hypernetwork, with the default weight initialization. For the parameters in the hypernetwork, a standard Kaiming initialization

Table S1: Specification of the hypernetwork used for each convolutional layer in our model, indexed by its depth in the network. A depth marked by * refers to the residual connection spanning across the specified layers. The characteristics of each layer is described in the format input-channels \times [kernel-size] \times output-channels under *Conv-layer*. Layers within the same group are generated by the same hypernetwork. Each hypernetwork has a unique parameter tensor of shape *Hnet-PS*, which, when multiplied by a layer and specialist-specific embedding of shape *Emb-PS* and reshaped appropriately, generates the primary network parameter of shape *Base-PS*.

Depth	Conv-layer	Base-PS	Layer group	Hnet-PS	Emb-PS
1	$3 \times [3 \times 3] \times 16$	[16, 3, 3, 3]	0	[16, 3, 3, 3, 10]	[10, 1]
2	$16 \times [3 \times 3] \times 160$	[160, 3, 3, 16]	1	[160, 3, 3, 16, 7]	[7, 1]
3	$160 \times [3 \times 3] \times 160$	[160, 3, 3, 160]	2	[160, 3, 3, 80, 14]	[14, 2]
4	$160 \times [3 \times 3] \times 160$	[160, 3, 3, 160]	2	[160, 3, 3, 80, 14]	[14, 2]
5	$160 \times [3 \times 3] \times 160$	[160, 3, 3, 160]	2	[160, 3, 3, 80, 14]	[14, 2]
6	$160 \times [3 \times 3] \times 160$	[160, 3, 3, 160]	2	[160, 3, 3, 80, 14]	[14, 2]
7	$160 \times [3 \times 3] \times 160$	[160, 3, 3, 160]	2	[160, 3, 3, 80, 14]	[14, 2]
8	$160 \times [3 \times 3] \times 160$	[160, 3, 3, 160]	2	[160, 3, 3, 80, 14]	[14, 2]
9	$160 \times [3 \times 3] \times 160$	[160, 3, 3, 160]	2	[160, 3, 3, 80, 14]	[14, 2]
10	$160 \times [3 \times 3] \times 320$	[320, 3, 3, 160]	3	[320, 3, 3, 160, 14]	[14, 1]
11	$320 \times [3 \times 3] \times 320$	[320, 3, 3, 320]	3	[320, 3, 3, 160, 14]	[14, 2]
12	$320 \times [3 \times 3] \times 320$	[320, 3, 3, 320]	3	[320, 3, 3, 160, 14]	[14, 2]
13	$320 \times [3 \times 3] \times 320$	[320, 3, 3, 320]	3	[320, 3, 3, 160, 14]	[14, 2]
14	$320 \times [3 \times 3] \times 320$	[320, 3, 3, 320]	3	[320, 3, 3, 160, 14]	[14, 2]
15	$320 \times [3 \times 3] \times 320$	[320, 3, 3, 320]	3	[320, 3, 3, 160, 14]	[14, 2]
16	$320 \times [3 \times 3] \times 320$	[320, 3, 3, 320]	3	[320, 3, 3, 160, 14]	[14, 2]
17	$320 \times [3 \times 3] \times 320$	[320, 3, 3, 320]	3	[320, 3, 3, 160, 14]	[14, 2]
18	$320 \times [3 \times 3] \times 640$	[640, 3, 3, 320]	4	[640, 3, 3, 320, 14]	[14, 1]
19	$640 \times [3 \times 3] \times 640$	[640, 3, 3, 640]	4	[640, 3, 3, 320, 14]	[14, 2]
20	$640 \times [3 \times 3] \times 640$	[640, 3, 3, 640]	4	[640, 3, 3, 320, 14]	[14, 2]
21	$640 \times [3 \times 3] \times 640$	[640, 3, 3, 640]	4	[640, 3, 3, 320, 14]	[14, 2]
22	$640 \times [3 \times 3] \times 640$	[640, 3, 3, 640]	4	[640, 3, 3, 320, 14]	[14, 2]
23	$640 \times [3 \times 3] \times 640$	[640, 3, 3, 640]	4	[640, 3, 3, 320, 14]	[14, 2]
24	$640 \times [3 \times 3] \times 640$	[640, 3, 3, 640]	4	[640, 3, 3, 320, 14]	[14, 2]
25	$640 \times [3 \times 3] \times 640$	[640, 3, 3, 640]	4	[640, 3, 3, 320, 14]	[14, 2]
2 \rightarrow 4*	$16 \times [1 \times 1] \times 160$	[160, 1, 1, 16]	5	[160, 1, 1, 16, 7]	[7, 1]
10 \rightarrow 12*	$160 \times [1 \times 1] \times 320$	[320, 1, 1, 160]	6	[320, 1, 1, 160, 7]	[7, 1]
18 \rightarrow 20*	$320 \times [1 \times 1] \times 640$	[640, 1, 1, 320]	7	[640, 1, 1, 320, 7]	[7, 1]

[61] is used, while the batch normalization (batchnorm) units are initialized with a weight and bias of 1 and 0, respectively.

Batch normalization units. Whenever we use averaged SGD, we follow Izmailov et al. [21] and perform a full pass over the training set to compute the batchnorm unit statistics before testing. This correction is required since the online batchnorm mean and variance estimates track the activations produced with the raw (non-averaged) weights during training, while the averaged solution is the one used when predicting at test time.

Learning rate schedule. As reported in the main text we use the multistep learning rate schedule employed in the original WRN paper [31] when optimizing with SGD. An initial learning rate of 0.1 is multiplied by a factor of 0.2 at the end of the 60th, 120th and 160th epochs. For Polyak-averaged SGD (ASGD), we follow [33, 21], who investigated ASGD training of WRNs, and linearly decrease the learning rate at every epoch starting at the end of the 80th epoch to the end of the 160th epoch. At the beginning of the 161st epoch, weight averaging is turned on and the learning rate is held constant at the final value of 0.05. Our minibatches contain 128 samples.

Data augmentation and preprocessing. All images are normalized channelwise by subtracting the mean and dividing by the standard deviation; both statistics are computed on the training dataset. The same transformation is then applied when testing, including to OOD data. Following a standard procedure [e.g., 31, 32] we augment our training datasets using random crops (with a 4-pixel padding) and random horizontal flips. Our OOD datasets are resized to fit whenever necessary; we used the resized images made available by Lee et al. [39].

Hyperparameters for SWAG, FGE, SE and IE. For SWAG, we use $N = 30$, following Maddox et al. [33]. For SE, we create $N = 10$ snapshots from the 164th epoch until the final one. The FGE results were directly reproduced from [6] and the authors used $N = 12$. Except for FGE, all methods (including ours) use the same learning rate schedule as SWAG, described above. The results for SWAG, SE, FGE and IE were all produced using a standard WRN 28-10 model, using the code provided in the repository of [33], that was in turn based on a public implementation which can be found here: <https://github.com/meliketoy/wide-resnet.pytorch>.

Hyperparameters for Table 1 and Table 2. For our economical ensemble, we generate $N = 10$ specialists at the end of epoch $T_0 = 120$. Furthermore, every specialist has its own set of dedicated batchnorm units, which are initialized at T_0 (batchnorm parameters, just like embeddings, are also perturbed with initialization noise amplitude $\sigma = 0.25$). Learning rate held constant at 0.1 when noted.

Hyperparameters for Fig. 2 and Table 2. All hyperparameters as described above except for the learning rate which is held constant at 0.1.

Hyperparameters for Table 3, Table 4 and Fig. 3. Here, we increase the initialization noise level to $\sigma = 0.5$ and we share the same batchnorm units across every specialist, as we found that this led to an improvement of OOD performance. All other hyperparameters as described above.

Table S2: Test set accuracy (in %, \pm standard deviation) and OOD performance, measured by the AUROC ($\times 100$, \pm standard deviation). We train our models (200 epochs, SGD and ASGD) on FashionMNIST (*FM*) and attempt to discriminate test set images from novel ones drawn from the MNIST, KMNIST and EMNIST (letters) dataset. Our ensembles (*Ours*, $N=10$) significantly improve the $N=1$ baseline and outperform all other economical ensembling methods considered here. Late-phase ensembling is crucial in improving against $N=1$, as evidenced by the poor result obtained when learning every specialist from scratch (*scratch*). Best results in boldface, excluding non-economical IEs (single seed).

Data	Optim.	Method	Test acc.	MNIST	KMNIST	EMNIST
FM	SGD	WRN ($N=1$)	95.41 \pm 0.16	97.21 \pm 0.34	95.77 \pm 1.21	96.87 \pm 0.26
		Ours ($N=1$)	95.49 \pm 0.02	97.41 \pm 0.41	97.21 \pm 0.50	97.16 \pm 0.38
		Ours	95.35 \pm 0.10	97.46 \pm 0.56	97.80 \pm 0.72	97.44 \pm 0.65
		IE	95.83	96.47	95.99	96.75
	ASGD	WRN ($N=1$)	95.61 \pm 0.08	95.42 \pm 0.97	94.76 \pm 1.39	94.45 \pm 0.94
		Ours ($N=1$)	95.56 \pm 0.08	95.13 \pm 0.27	94.08 \pm 0.75	93.79 \pm 0.79
		Ours (scratch)	95.66 \pm 0.10	96.38 \pm 0.55	96.38 \pm 0.15	95.26 \pm 0.44
		SWAG	95.45 \pm 0.02	95.48 \pm 0.53	93.99 \pm 0.25	95.47 \pm 0.51
		SE	95.62 \pm 0.09	95.35 \pm 0.88	94.66 \pm 1.55	94.43 \pm 1.05
		Late IE	95.31 \pm 0.04	93.72 \pm 0.92	93.64 \pm 0.81	92.78 \pm 0.94
		Ours	95.72 \pm 0.07	96.65 \pm 0.68	96.45 \pm 0.87	95.96 \pm 0.78
		IE	95.79	95.39	95.00	94.33

C Additional experiments

We now describe a series of additional experiments and control studies which complement our main text results. As in the main text, we always report mean and standard deviation across three random seeds.

Table S3: Test set accuracy (in %, \pm standard deviation) and OOD performance, measured by the AUROC ($\times 100$, \pm standard deviation). We train our models (200 epochs with ASGD) on CIFAR-10 (*C10*) and CIFAR-100 (*C100*) and attempt to discriminate test set images from novel ones drawn from the SVHN, LSUN, Tiny ImageNet (*TIN*) and the resp. other CIFAR dataset. We compare different σ and observe a trade-off behaviour between accuracy and OOD AUROC where too much noise results in lower test set accuracies while OOD performance degrades when pushing too gently ($\sigma \in \{0.0, 0.25\}$).

Data	Optim.	Method	Test acc.	SVHN	LSUN	TIN	CIFAR
C10	ASGD	$\sigma=0.0$	96.57 \pm 0.29	98.68 \pm 0.28	96.97 \pm 0.08	95.44 \pm 0.29	92.94 \pm 0.12
		$\sigma=0.25$	96.47 \pm 0.10	98.78 \pm 0.07	97.17 \pm 0.07	95.75 \pm 0.09	93.10 \pm 0.18
		$\sigma=0.5$	96.48 \pm 0.02	99.07 \pm 0.04	97.53 \pm 0.04	96.11 \pm 0.13	93.36 \pm 0.15
		$\sigma=0.75$	96.50 \pm 0.03	98.98 \pm 0.28	97.68 \pm 0.22	96.27 \pm 0.43	93.36 \pm 0.10
		$\sigma=1.0$	96.42 \pm 0.14	99.16 \pm 0.10	97.99 \pm 0.16	96.79 \pm 0.20	93.39 \pm 0.10
C100	ASGD	$\sigma=0.0$	82.62 \pm 0.14	86.40 \pm 0.87	79.66 \pm 2.22	77.80 \pm 2.63	81.41 \pm 0.59
		$\sigma=0.25$	82.76 \pm 0.29	86.52 \pm 1.84	80.80 \pm 3.25	79.14 \pm 2.61	81.69 \pm 0.52
		$\sigma=0.5$	82.55 \pm 0.13	86.67 \pm 1.28	86.58 \pm 2.96	85.54 \pm 3.01	81.71 \pm 0.23
		$\sigma=0.75$	82.63 \pm 0.49	83.91 \pm 0.82	85.72 \pm 0.71	84.91 \pm 0.97	81.82 \pm 0.23
		$\sigma=1.0$	82.44 \pm 0.31	83.16 \pm 1.42	84.88 \pm 1.39	84.54 \pm 2.00	81.90 \pm 0.49

C.1 Fashion-MNIST OOD experiments

We reproduced the experiments reported in the main text, now training on the Fashion-MNIST dataset [27] (Table S2). We set the hyperparameters to the values used for the CIFAR datasets and repeat the OOD experiment on MNIST [62], K-MNIST [63] and E-MNIST letters [64]. Similar to the results obtained on CIFAR-10 and CIFAR-100, we see an improvement on AUROC values across all out-of-distribution datasets while also raising test set accuracy. As in the main text results, ours as well as all related methods (except from independent ensembles, IEs) were trained for 200 epochs on a WRN 28-10 model, while approximately conserving the number of parameters.

C.2 Different ensembling timing T_0 and initialization noise σ

We investigate our two main new hyperparameters, the initialization noise amplitude σ and timing T_0 , on the CIFAR datasets. For both hyperparameters, we observe a trade-off behavior between OOD performance and predictive accuracy. Diversity can be enhanced by injecting more noise in the ensemble initialization, or by moving the initialization to a later phase of training. This leads to an increase in AUROC values across the novel datasets, but seems to harm test set accuracy. For all results shown in Table S3 and Table S4, we use the same hyperparameters (except from σ , T_0) used for obtaining the results of Table 4 in the main text. We choose to report $T_0 = 120$ in the main text as a compromise setting across datasets.

Table S4: Test set accuracy (in %, \pm standard deviation) and OOD performance, measured by the AUROC ($\times 100$, \pm standard deviation). We train our models (200 epochs with ASGD) on CIFAR-10 (*C10*) and CIFAR-100 (*C100*) and attempt to discriminate test set images from novel ones drawn from the SVHN, LSUN, Tiny ImageNet (*TIN*) and the resp. other CIFAR dataset. We compare different ensemble initialization times T_0 and observe a trade-off behavior between accuracy and AUROC when initialization is too late (or, respectively, too early). This effect is more pronounced on CIFAR-100.

Data	Optim.	Method	Test acc.	SVHN	LSUN	TIN	CIFAR
C10	ASGD	$T_0=80$	96.55 ± 0.05	99.17 ± 0.14	97.59 ± 0.13	96.17 ± 0.27	93.34 ± 0.10
		$T_0=120$	96.48 ± 0.02	99.07 ± 0.04	97.53 ± 0.04	96.11 ± 0.13	93.36 ± 0.15
		$T_0=160$	96.43 ± 0.11	98.95 ± 0.13	97.47 ± 0.34	96.14 ± 0.37	93.37 ± 0.02
C100	ASGD	$T_0=80$	82.66 ± 0.24	87.15 ± 2.86	81.27 ± 3.42	81.66 ± 3.34	82.02 ± 0.09
		$T_0=120$	82.55 ± 0.13	86.67 ± 1.28	86.58 ± 2.96	85.54 ± 3.01	81.71 ± 0.23
		$T_0=160$	82.70 ± 0.19	88.08 ± 0.90	83.86 ± 2.40	83.17 ± 1.70	81.98 ± 0.23

C.3 Training for 300 epochs

In this section, we explore the performance of our economical ensemble when increasing the number of training epochs by a factor of $1.5\times$, using ASGD. Such an increase in training budget is commonly allowed in economical learning studies [e.g., 33]. Here, we decrease the learning rate linearly from the 80th epoch to the end of the 240th epoch, and we set $T_0 = 160$. All other hyperparameters are left unchanged. Training for 300 epochs leads to improved predictive accuracy on both CIFAR datasets (Table S5), in particular on CIFAR-100.

Table S5: Test set accuracies (in %, \pm standard deviation) when training (for 300 epochs) on CIFAR-10/100 (*C10*, *C100*). All models perform generally better than when training for 200 epochs, while our ensembling method (*Ours*, learned with nested ASGD) still outperforms the baseline (*Ours* $N=1$, learned with ASGD) as well as other state-of-the-art economical methods (*SWAG*). Best results in boldface.

	WRN ($N=1$)	Ours ($N=1$)	Ours	SWAG	Ours (200)
C10	96.43 \pm 0.12	96.55 \pm 0.10	96.87 \pm 0.08	96.25 \pm 0.08	96.79 \pm 0.07
C100	82.49 \pm 0.07	82.61 \pm 0.40	83.30 \pm 0.25	82.42 \pm 0.19	83.03 \pm 0.33

C.4 Larger residual networks

In the main text we present results for the popular WRN 28-10 configuration of the wide residual network model. Here we complement our results with simulations of two larger models of the same family, the WRN 28-14 and the WRN-18. To make use of the additional capacity afforded by such models, we train for 300 epochs and use an additional data augmentation procedure known as cutout [36]. The stronger performance that we obtain (Table S6) demonstrate the ability of our algorithm to scale to architectures with larger numbers of parameters.

Table S6: Test set accuracies (in %) when training larger WRN models for 300 epochs on CIFAR-10/100 (*C10*, *C100*) with an additional data augmentation procedure (cutout; [36]). Again, the predictive accuracy of the baseline (*Ours* $N=1$, learned with averaged SGD) is again significantly improved using our ensembling method (*Ours*, learned with nested averaged SGD, $N=10$, initialization noise $\sigma = 0.25$ for *C10* and $\sigma = 0.5$ *C100*). For all models we started annealing the learning rate (initially set to 0.1) at epoch 80 until epoch 240 with a final learning rate of $\sigma = 0.01$ for *C10* and $\sigma = 0.05$ *C100* for the last 60 epochs.

	WRN ($N=1$)	Ours ($N=1$)	Ours	Params.
C10 - WRN 28-14	97.15 \pm 0.08	97.31 \pm 0.05	97.56 \pm 0.06	\sim 70.5Mio
C10 - WRN 28-18	97.20 \pm 0.05	97.42 \pm 0.04	97.62 \pm 0.08	\sim 117.5Mio
C100 - WRN 28-14	83.79 \pm 0.15	84.41 \pm 0.35	85.55 \pm 0.24	\sim 70.6Mio
C100 - WRN 28-18	84.44 \pm 0.16	84.88 \pm 0.23	85.91 \pm 0.15	\sim 118.2Mio

C.5 Different ensemble sizes

We investigate different sizes of our economical ensemble under the hyperparameter setting used to produce Table 3. We observe comparable performance when varying N , keeping all other hyperparameters (tuned for $N=10$) fixed, Table S7.

C.6 Lower learning rate experiments

In the main text we studied nesting SGD updates over shared and specialist-specific parameters to stabilize ensemble learning. A straightforward alternative is to simply lower the overall learning rate across both parameter types. We investigate this option here and set the final learning rate values to 0.01 instead of 0.05 (we recall that we used 0.05 as the final learning rate to produce the results reported in Table 1). We find that a simple lowering of the learning rate does not result in better predictive accuracy on either of the CIFAR datasets, Table S8.

Table S7: Test set accuracy (in %, \pm standard deviation) and OOD performance, measured by the AUROC ($\times 100$, \pm standard deviation). We train our models (200 epochs with ASGD) on CIFAR-10 (*C10*) and CIFAR-100 (*C100*) and attempt to discriminate test set images from novel ones drawn from the SVHN, LSUN, Tiny ImageNet (*TIN*) and the resp. other CIFAR dataset. We compare other ensemble sizes ($N=5, 10, 15$) with the setup used to produce results reported in Table 4 of the main text. Overall, $N=10$ produces the best accuracies across datasets.

Data	Optim.	Method	Test acc.	SVHN	LSUN	TIN	CIFAR
C10	ASGD	$N=5$	96.50 ± 0.09	99.06 ± 0.07	97.40 ± 0.10	98.14 ± 0.09	93.27 ± 0.11
		$N=10$	96.48 ± 0.02	99.07 ± 0.04	97.53 ± 0.04	96.11 ± 0.13	93.36 ± 0.15
		$N=15$	96.54 ± 0.03	98.86 ± 0.26	97.40 ± 0.17	96.02 ± 0.32	93.34 ± 0.07
C100	ASGD	$N=5$	82.61 ± 0.16	86.53 ± 2.16	82.17 ± 2.88	81.37 ± 3.11	81.89 ± 0.26
		$N=10$	82.55 ± 0.13	86.67 ± 1.28	86.58 ± 2.96	85.54 ± 3.01	81.71 ± 0.23
		$N=15$	82.55 ± 0.58	86.40 ± 1.26	85.59 ± 1.49	84.52 ± 1.20	81.54 ± 0.91

Table S8: Test set accuracy (in %, \pm standard deviation) and OOD performance, measured by the AUROC ($\times 100$, \pm standard deviation). We train our models (200 epochs with ASGD) on CIFAR-10 (*C10*) and CIFAR-100 (*C100*) with different final learning rates. We then attempt to discriminate test set images from novel ones drawn from the SVHN, LSUN, Tiny ImageNet (*TIN*) and the resp. other CIFAR dataset.

Data	Optim.	Learn. rate	Test acc.	SVHN	LSUN	TIN	CIFAR
C10	ASGD	$\eta=0.01$ ($N=1$)	96.71 ± 0.09	97.58 ± 0.14	95.88 ± 0.61	93.67 ± 0.74	90.81 ± 0.24
		$\eta=0.01$	96.68 ± 0.10	97.89 ± 0.34	96.01 ± 0.18	93.95 ± 0.26	90.65 ± 0.35
		$\eta=0.05$	96.44 ± 0.05	98.66 ± 0.27	96.97 ± 0.05	95.42 ± 0.10	93.07 ± 0.14
	NASGD	$\eta=0.01$	96.41 ± 0.18	95.16 ± 0.92	95.17 ± 0.31	92.70 ± 0.78	89.69 ± 0.17
		$\eta=0.05$	96.79 ± 0.07	97.38 ± 0.48	95.56 ± 0.40	93.02 ± 0.96	90.13 ± 0.43
C100	ASGD	$\eta=0.01$ ($N=1$)	82.31 ± 0.29	83.41 ± 4.07	$82.28 \pm 0.2.17$	79.89 ± 2.37	82.36 ± 0.13
		$\eta=0.01$	82.60 ± 0.20	81.19 ± 3.86	83.31 ± 2.32	81.68 ± 1.63	82.42 ± 0.13
		$\eta=0.05$	82.76 ± 0.24	84.79 ± 1.80	81.12 ± 1.13	80.21 ± 0.79	81.89 ± 0.05
	NASGD	$\eta=0.01$	82.00 ± 0.29	78.79 ± 2.72	83.49 ± 1.27	80.86 ± 1.70	81.64 ± 0.37
		$\eta=0.05$	83.03 ± 0.33	82.21 ± 1.40	82.03 ± 2.97	80.18 ± 3.14	82.67 ± 0.10

C.7 Nested SGD without weight averaging

In this section, we investigate if nested SGD (NSGD) can result in improved predictive accuracy when combined with standard SGD, with Polyak-averaging disabled. We follow the exact same training procedure used to produce results for Table 2 of the main text but compare SGD and nested SGD (both without Polyak-averaging). Although NASGD (with Polyak-averaging) outperforms NSGD, we again see a consistent increase in performance when nesting the update steps, Table S9. In this experiment, we change the learning rate annealer to start after epoch 80 and end at epoch 190 with a final learning rate of 0.001.

Table S9: Ensemble test set classification accuracy (in %, \pm standard deviation) when $N = 10$. Nested SGD (NSGD) leads to a consistent improvement in predictive accuracy, when compared to standard SGD alone (SGD; without Polyak-averaging) on Fashion-MNIST and CIFAR-10/100.

	Ours (SGD)	Ours (NSGD)
FM	95.49 \pm 0.15	95.57 \pm 0.03
C10	96.23 \pm 0.04	96.38 \pm 0.05
C100	81.61 \pm 0.23	82.01 \pm 0.07

C.8 Further compression gains

Following the original idea of Ha et al. [8] of reducing the number of trainable parameters in a deep neural network through hypernetworks, we investigated the effects of varying the dimensions of the shared hypernetwork parameters Θ . In this case, we not only aim to compress over the ensemble but also within a single model. Similar to [10], we observe a marginal decrease of performance on predictive accuracy (Table S10) as well as on OOD (Table S11). We note that we do not perform a new hyperparameter search optimizing for the new architecture; we use the hyperparameters that produced the results for Table 1 and Table 3 in the main text.

Table S10: Test set accuracies (in %, \pm standard deviation) when training for 200 epochs on CIFAR-10/100 (C10, C100) datasets. Compressing the number of trainable parameters through the hypernetwork leads to little decrease in test set accuracies.

No. of parameters:	15.6Mio	35.9Mio
C10	96.71 \pm 0.14	96.79 \pm 0.07
C100	82.51 \pm 0.20	83.03 \pm 0.33

C.9 Last-layer+batchnorm ensemble performance

To further confirm the contribution of our hypernetwork-embedded models in improving ensemble performance, we perform an ablation study in which we keep a single set of weight embeddings E_0 and only generate N specialist-specific last-layer weights and N specialist-specific batchnorm units. This is a simpler economical ensemble, an extreme form of TreeNet [15] paired with our late-phase ensembling, which already results in improved performance in both predictive accuracy (Table S12) and OOD (Table S13; here a single set of ensemble-shared batchnorm units is used, as in Table 3).

Table S11: Test set accuracy (in %, \pm standard deviation) and OOD performance, measured by the AUROC ($\times 100$). We train our models (200 epochs with ASGD) on CIFAR-10 (*C10*) and CIFAR-100 (*C100*) and attempt to discriminate test set images from novel ones drawn from the SVHN, LSUN, Tiny ImageNet (*TIN*) and the resp. other CIFAR dataset. By varying the size of shared parameters Θ , we can control and compress the number of trainable parameters. We observe a modest decline on CIFAR-10 test set accuracy, while the difference is more significant for CIFAR-100. OOD performance remains remarkably strong across experiments.

Data	Param.	Test acc.	SVHN	LSUN	TIN	CIFAR
C10	15.6Mio	96.33 ± 0.05	99.08 ± 0.31	97.89 ± 0.23	96.75 ± 0.50	93.33 ± 0.10
	35.9Mio	96.48 ± 0.02	99.07 ± 0.04	97.53 ± 0.04	96.11 ± 0.13	93.36 ± 0.15
C100	15.6Mio	81.67 ± 0.17	84.00 $\pm 0.3.80$	86.05 ± 0.88	85.73 ± 1.39	82.10 ± 0.48
	35.9Mio	82.55 ± 0.13	86.67 ± 1.28	86.58 ± 2.96	85.54 ± 3.01	81.71 ± 0.23

Table S12: Test set accuracies (in %, \pm standard deviation) when training for 200 and 300 epochs on CIFAR-10/100 (*C10*, *C100*) datasets. We took the hyperparameters used to produce Tables 1 and S5 (for 200- and 300-epoch learning, resp.). LL+BN is a stripped down economical ensemble where only the last-layer weights and batchnorm units are specialist-specific.

		Test acc. (@ epoch 200)	Test acc. (@ epoch 300)
C10	LL+BN	96.81 ± 0.12	96.77 ± 0.13
	Ours	96.79 ± 0.07	96.87 ± 0.08
C100	LL+BN	82.82 ± 0.09	83.07 ± 0.05
	Ours	83.03 ± 0.33	83.30 ± 0.25

Table S13: Test set accuracy (in %, \pm standard deviation) and OOD performance, measured by the AUROC ($\times 100$, \pm standard deviation). We train our models (200 epochs with ASGD) on CIFAR-10 (*C10*) and CIFAR-100 (*C100*) and attempt to discriminate test set images from novel ones drawn from the SVHN, LSUN, Tiny ImageNet (*TIN*) and the resp. other CIFAR dataset. We set the hyperparameters to those used to produce Table 3. LL is a stripped down economical ensemble where only the last-layer weights are specialist-specific (here, batchnorm units are ensemble-shared, as in our main text OOD experiments).

Data	Model	Test acc.	SVHN	LSUN	TIN	CIFAR
C10	LL	96.45 ± 0.03	98.72 ± 0.02	96.66 ± 0.21	95.30 ± 0.36	92.96 ± 0.04
	Ours	96.48 ± 0.02	99.07 ± 0.04	97.53 ± 0.04	96.11 ± 0.13	93.36 ± 0.15
C100	LL	82.69 ± 0.03	87.32 ± 1.39	82.42 ± 4.36	79.83 ± 3.28	81.78 ± 0.22
	Ours	82.55 ± 0.13	86.67 ± 1.28	86.58 ± 2.96	85.54 ± 3.01	81.71 ± 0.23

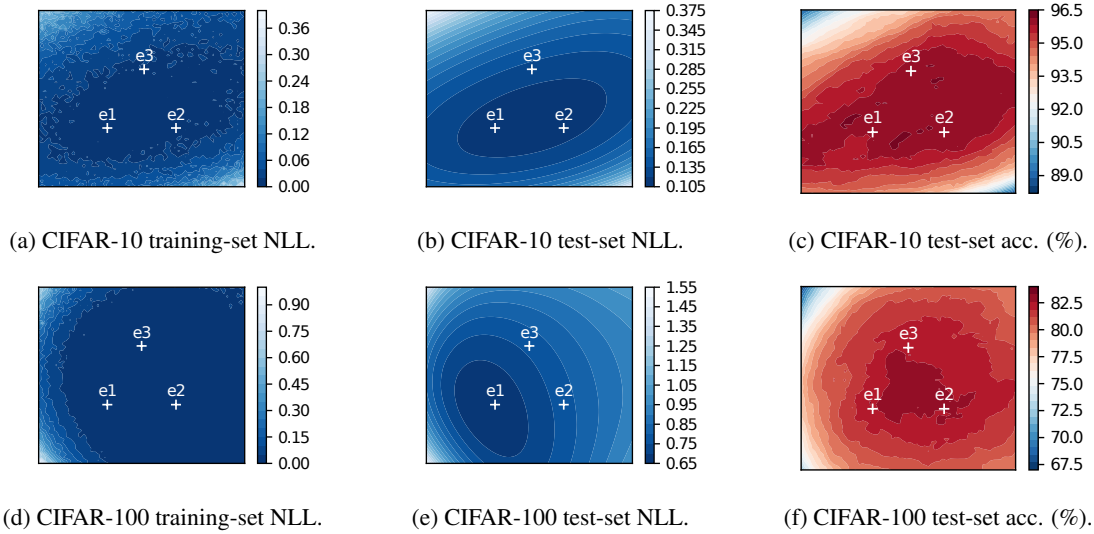


Figure S2: Embedding space visualizations ($N = 10$, OOD-optimized ensemble learned with ASGD) on a plane defined by three specialist embeddings (denoted by crosses). We use 2048 examples when estimating the accuracy and NLL on the test set and 512 examples when estimating the NLL on the training set. The reported NLL values are per-example averages.

C.10 Additional visualizations in embedding space

Lastly, we provide additional embedding space visualizations (Fig. S2) accompanying our main text Fig. 3. The flatness and centering of the learned weight embeddings is apparent, particularly in the negative log-likelihood (NLL) estimated over the training set, our loss function \mathcal{L} .

D Scientific computing environment

We wrote custom code in Python 3.7 using the automatic differentiation and GPU acceleration package PyTorch (version 1.4.0) to simulate our models. We used the standard datasets (including training and test splits) as provided by the torchvision package unless stated otherwise. All plots were produced using matplotlib [65]. We ran our experiments on Linux workstations equipped with multiple NVIDIA GeForce 2080 Ti GPUs.

E Code forks

Some elements of our hypernetwork implementation were inspired on the code that was made publicly available by Savarese and Maire [10]. Our implementation of averaged SGD was adapted from the code accompanying the work of Izmailov et al. [21], now available on the torchcontrib python package. The SWAG method was evaluated directly using the code provided by the authors [33]. Finally, we used the same base WRN model as [33].